Environmental Science and Pollution Research (2023) 30:8448–8463
https://doi.org/10.1007/s11356-022-18835-6

RECENT INNOVATIONS IN CLEAN AND GREEN CONVERSION TECHNOLOGIES DEALING WITH AIR, WATER, BIOMASS, AND SOIL

Effect of experimental parameters on photocatalytic degradation efficiency of TiO_2 nanoparticles synthesized by electrochemical method towards Rhodamine B dye solution under natural sunlight

Shalini Vishwanathan[1] · Sree Laxmi[1] · Sukanya Nandan[1] · Shoni Jayan[1] · Meghna Lijo[1] · Susmita Das[1]

Received: 3 September 2021 / Accepted: 20 January 2022 / Published online: 5 February 2022

Abstract
In this study, ~ 40 nm anatase TiO_2 nanoparticles were successfully prepared by a simple electrochemical method by using succinic acid as a non-ammonia-based electrolyte solution and titanium sheets as electrodes. The effect of experimental parameters such as conductivity (2–12 mS/cm), pH of the initial solution (5–9), current applied (0.05–2 A), and reaction time (1–4 h) on catalyst productivity has been investigated. The analysis shows that at an optimum conductivity of 8 mS/cm and pH 7, an increase in applied current and reaction time maximizes the productivity of TiO_2 nanoparticles. The obtained catalyst was used for photocatalytic degradation of rhodamine B (RhB) under natural sunlight irradiation. The effect of experimental parameters on photocatalytic degradation has also been studied. The result displayed that degradation efficiency was enhanced by ~ 3 times in the alkaline region compared to the normal pH condition and increased with an increase in catalyst loading and decreased with the initial concentration of RhB dye. Investigation of the photocatalytic mechanism by radical trapping experiments showed that RhB photocatalytic degradation was mainly dominated by hole and superoxide radicals, whereas hydroxyl radical plays a minor role. Moreover, the catalyst reusability analysis revealed good stability and showed excellent degradation up to four consecutive cycles with nearly negligible loss of photocatalytic efficiency. Thus, the present work offers a new opportunity in terms of maximization of productivity as well as sunlight-driven photocatalytic activity of the catalyst for their industrial application.

Keywords Electrochemical method · Succinic acid · TiO_2 nanoparticles · Natural sunlight · Photocatalyst

Introduction

Nanostructured metal oxide semiconductor solar photocatalyst has gained the attention of several researchers due to its various unique characteristics features. Among all metal oxide semiconductor photocatalysts, titanium dioxide (TiO_2) has been extensively studied for the removal of recalcitrant pollutants like dyes, pesticides, and pharmaceutical wastes in wastewater treatment (Saouda et al. 2017; Zeghioud et al. 2019). TiO_2 has three polymorphs states as anatase, rutile, and brookite with separate bandgap energies of 3.2 eV, 3.0 eV, and ~3.2 eV, respectively. The wide spectra of applications of TiO_2 as a photocatalyst are owing to its super hydrophilicity, chemical stability, strong oxidizing power, and visible light transparency properties (Nakata and Fujishima 2012; Hajjaji et al. 2018). The excellent qualities such as nontoxicity, low cost, biocompatibility, and earth abundance make TiO_2 the most important photocatalyst with industrial applications in the present and near-future scenarios (Dal Santo and Naldoni 2018; Zeghioud et al. 2018). Hence, investigating a simple, direct, and new method to synthesize TiO_2 photocatalyst is of academic and industrial importance. Also, a synthesis method that emphasizes the industrial scale-up possibilities with a maximum yield of catalyst would open numerous prospectus for practical applications. In general, synthesis techniques such as precipitation, sol–gel method, hydrothermal, polyol synthesis, etc.

Responsible Editor: Sami Rtimi

✉ Susmita Das
susmita.82.das@gmail.com

[1] Department of Chemical Engineering, National Institute of Technology Calicut, Calicut-673601, India

had been used for the synthesis of TiO_2 nanoparticles (Kang et al. 2016; Gomathi Thanga Keerthana et al. 2018; Tripathy et al. 2009). The disadvantages inherent to the precipitation method, such as the inefficiency to produce high purity crystalline nanoparticles, nonuniformity in size and shape, and batch to batch production variation, limit its practical applications. In the sol–gel method, aging of the gel and removal of surfactant after reaction increases the time of nanoparticle synthesis (Carter and Norton 2007). Removal of surfactant by several repetitive washing may affect the physical properties of nanoparticles. The hydrothermal method is widely practiced due to the versatility of the technique to ensure the control of the nucleation and growth characteristics of the nanomaterial but the secondary treatment to remove the template makes the method less approachable (Rane et al. 2018). Although the polyol process yields high purity residual free nanopowders through low-temperature synthesis, the reducing properties of the polyols can cause the production of elemental metals in place of metal oxides during the synthesis (Dong et al. 2015). Overall, the conventional TiO_2 synthesis methods are time consuming and consist of multiple processes. On the other hand, the electrochemical synthesis process is easy, economical, and simple for scale-up for industrial-level nanoparticles production (Das and Srivastava 2017). In this process, a small amount of electrical energy or current has been passed through the metal sheet, which acts as a sacrificial anode to produce metallic cations, which are further oxidized by the water oxidation process and produce metal oxide. Properties of obtained particles could be controlled by current density and electrolyte bath composition. This process is much more suitable for synthesizing highly pure metal oxide particles with a high surface area. Obtained particles could be easily separated from the reactant solution as no other reagent is involved.

Extensive information is available on the synthesis of TiO_2 nanotube (TNT) arrays by the electrochemical method. The main disadvantage of the electrochemical method is the detachment of the nanotubes from the substrate, which requires further downstream processing (Roy et al. 2011). Several reports have also been observed on TiO_2 thin film production in the electrochemical method by cathodic deposition techniques. In the cathodic deposition technique, the agglomerated TiO_2 nanoparticles formed thin films on the cathode. Subsequently, these films are either scratched out of the cathode for further processing, or the cathode is directly annealed for crystallization of the film. The nanofilms produced by this method generally have less surface area available for application purposes. In this context, the synthesis of dispersed TiO_2 nanoparticles by electro-oxidation method has been rarely reported, and the studies focusing on the overall productivity of the catalyst are even scarce. Researchers have mostly used ammonia-based electrolyte solutions such as tetrabutylammonium bromide and the mixture of tetra propyl ammonium bromide salt, tetrahydrofuran, and acetonitrile for the synthesis of TiO_2 nanoparticles by electro-oxidation method (Anandgaonker et al. 2015; Bezares et al. 2015). Disposal of these ammonia-based electrolyte solutions after the reaction is extremely hazardous to the environment. The selection of a non-ammonia-based, eco-friendly, and inexpensive electrolyte solution is therefore advantageous to the industrial production of nanoparticles by electrochemical method. To the best of our knowledge, no studies have been carried out on the synthesis of TiO_2 nanoparticles through the galvanostatic electro-oxidation method by using the non-ammonia-based aqueous succinic acid solution and its productivity maximization as well as utilization for natural sunlight-driven photocatalytic applications.

Based on the above discussion, we have successfully prepared TiO_2 nanoparticles by an electrochemical method by using aqueous succinic acid and titanium sheets as the electrolyte and electrodes, respectively. The obtained TiO_2 nanoparticles were characterized by using several characterization techniques. Our work aims to synthesize TiO_2 nanoparticles by using non-ammonia-based aqueous succinic acid as an electrolyte solution and to study the influence of operating parameters to optimize for maximum productivity of TiO_2 nanoparticles. The photocatalytic efficiency of the obtained catalyst was explored by degrading RhB dye under natural sunlight irradiation. The UV fraction of the natural sunlight spectrum is mainly responsible for the photocatalytic activity of TiO_2 nanoparticles. Moreover, another goal of the present work is to analyze the effect of the catalyst dose, pH of initial dye solution, and dye concentration on photocatalytic degradation of RhB. In addition to a plausible photocatalytic mechanism of the TiO_2 catalyst, scavengers study showed that hole and superoxide radicals are key controlling parameters for photocatalytic degradation of RhB. The presence of oxygen vacancies and surface defects as described by PL spectra confirms the better charge separation in TiO_2 catalyst, which enhances the degradation efficiency. We have succeeded in re-using the TiO_2 catalyst up to 4 cycles without any loss of photocatalytic activity, which shows its potential application in industrial wastewater treatment. We have also conducted adsorption studies to verify that the removal of RhB via adsorption remains very small.

Materials and methods

All chemicals such as succinic acid ($C_4H_6O_4$, > 99 wt%), sodium hydroxide pellets (NaOH, > 97 wt%), nitric acid (HNO_3, 69 wt%), and potassium chloride (KCL, 99.8 wt%) were purchased from Sigma-Aldrich. Titanium sheets of 2.4 mm thickness were purchased from Norrust Electro Tech, Chennai. Ultrapure water (18 MΩ cm) was used for

all experimental purposes. All the reagents were used without further purification.

Fabrication of TiO_2 nanoparticles

TiO_2 nanoparticles were synthesized by using a 0.15 M aqueous succinic acid electrolyte solution. The pH and conductivity of the electrolytic solution were maintained by utilizing 1 M NaOH and KCL solution. Electrochemical experiments were performed by immersing the titanium electrode by keeping a gap of 1.5 cm between the electrodes within a glass electrolyte cell. The exposed dimension of titanium foil was about $2 \times 2 \times 0.2$ cm^3 for all the experiments. A direct current power source was used to supply the current to the electrodes. The experiment was conducted at a constant agitation speed of 300 rpm. The colloidal precipitated particles were collected by centrifuging and washing with DI water to remove any un-reacted reactants. The obtained nanoparticles were dried at 60 °C for 24 h, subsequently followed by calcination at 500 °C for 5 h within a muffle furnace. Finally, the white color powder sample was collected and used for various characterizations. After each experiment, electrodes were cleaned with an aqueous 10% nitric acid solution and distilled water for reuse.

Characterization

Different analysis was done to identify the obtained compound. FTIR spectra were recorded by FTIR spectroscope (Thermo Nicolet 6700, NEXUS, USA). X-ray diffraction analysis (XRD) was done to carry out a crystallographic phase analysis of the photocatalyst by using a Bruker AXS/D8 diffractometer. Thermogravimetric analysis (TGA) was performed in EX STAR 6300 instrument from room temperature to 1000 °C. The surface morphology of TiO_2 nanoparticles was analyzed by FE-SEM techniques (QUANTA, Model 200 FEG, Netherland). The elemental distribution of the obtained sample was analyzed by EDX analysis. FEI Tecnai G2 20 S-Twin machine was used to record TEM images. UV–vis diffuse reflectance spectra (UV–vis DRS) were recorded by model UV-2450, SHIMADZU instrument to analyze the optical properties and the bandgap of the samples within a wavelength range of 200–800 nm. BELSORP-mini II (BEL. Japan Inc) surface area and porosity analyzer at – 197 °C were used to analyze the textural properties of the catalyst. The specific surface area of the obtained sample was determined by Brunauer–Emmett–Teller (BET) surface area method by analyzing multipoint nitrogen adsorption–desorption isotherms. The pore size distribution of catalyst was analyzed from the adsorption isotherm using Barrett–Joyner–Halenda (BJH) method. Room temperature photoluminescence spectra of the synthesized catalyst were collected using a PerkinElmer LS45 fluorescence spectrometer at an excitation wavelength of 300 nm. UV spectrophotometer, model UV-1800, Shimadzu, was used for the analysis of the degradation efficiency of RhB dye solution.

Photocatalytic activity and adsorption experiments

The photocatalytic degradation efficiency of TiO_2 nanoparticles was analyzed by degrading RhB dye solution under natural sunlight. The experiments were performed by preparing a known concentration of aqueous dye solutions with a particular amount of catalyst loading. The mixture of dye solution and catalyst was placed under dark with stirring for 30 min to attain the adsorption–desorption equilibrium, subsequently, the mixture was irradiated by natural sunlight for degradation. Before starting the adsorption–desorption equilibrium, the solution was maintained at a particular pH. During the photocatalytic experiment, 3 ml aliquot was withdrawn at a regular interval of 30 min and continued till the dye was completely degraded into a colorless solution. The photocatalytic degradation efficiency of RhB was examined at $\lambda_{max} = 554$ nm. The degradation efficiency η (%) was calculated by using Eq. 1:

$$\%\text{Degradationefficiency}(\eta) = \frac{C_0 - C}{C_0} \times 100 \quad (1)$$

where $\boldsymbol{c}_0$ and $\boldsymbol{c}$ denote the concentration of RhB dye at initial and different irradiation time, respectively.

Scavenger study was carried out by adding 6 mM of scavengers such as ethylene diamine tetraacetic acid (EDTA), isopropyl alcohol (IPA), and ascorbic acid (AA) to 5 mg/L RhB solution at 1 g/L TiO_2 catalyst loading at pH 12. Furthermore, the dye solution was irradiated under sunlight for 240 min, and a 3 mL aliquot was withdrawn every 30 min interval. The collected sample was centrifuged repeatedly to eliminate the suspended photocatalyst. The dye solution concentration was measured by a UV–visible spectrophotometer.

The adsorption experiments for the removal of RhB dye were performed in a batch process where a 100 mL flask containing 25 mL mixture of known concentration dye solution with a catalyst loading was kept within an orbital shaker incubator. All the experiments were performed at a shaking speed of 100 rpm and allowed sufficient time to reach adsorption equilibrium. At the end of the adsorption process, the solution was centrifuged to eliminate any suspended catalyst. The RhB dye solution concentration was measured by a UV–visible spectrophotometer at $\lambda_{max} = 554$ nm. The amount of dye adsorption onto TiO_2 catalyst at equilibrium, q_e (mg/g), was obtained as follows:

$$q_e = \frac{c_o - c_e}{m} \times V \quad (2)$$

where c_0 and c_e represents the concentration of RhB dye solution at initial and equilibrium conditions (mg/L), respectively. V is the volume of the dye solution (L) and m is the weight of the adsorbent used (g).

Result and discussion

The surface morphology of the TiO_2 nanoparticles was analyzed by performing SEM and TEM techniques, as shown in Fig. 1A and 1B. The analysis shows that obtained samples are a cluster of nanoparticles of ~ 40 nm diameter.

To explore the elemental distribution of the samples, EDX and elemental dot mapping analyses were carried out. The EDX analyses result for pure TiO_2 is shown in Fig. 2, along with point EDX data. Result illustrated that the major peaks corresponded to the Ti and O elements. The absence of any other peak confirmed the purity of the samples, as shown in Fig. 2B. The obtained result was reaffirmed by performing point EDX analysis, as shown in Fig. 2C. At three different points, EDX data was collected, and the result is displayed in Fig. 2C. The analysis revealed that every point within the sample shows the existence of titanium and oxygen, which shows the uniformity of the obtained sample. Furthermore, the EDX elemental dot-mapping images of the obtained sample have been shown in Fig. 2A. The results

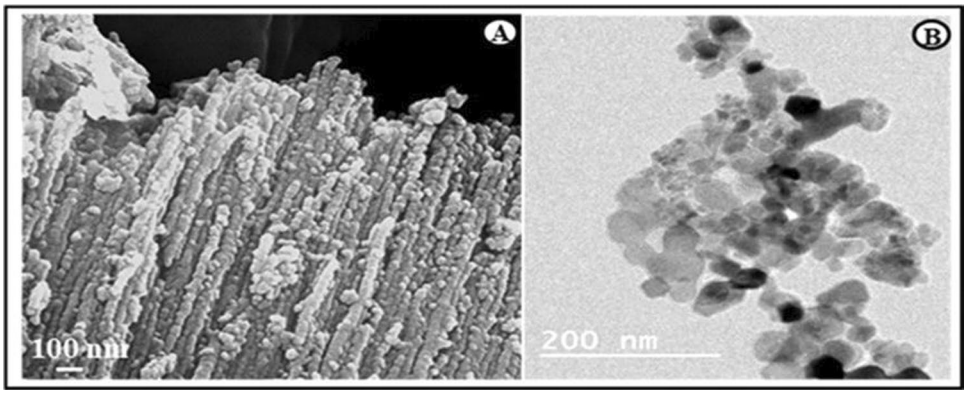

Fig. 1 **A** SEM image of TiO_2 nanoparticles synthesized by electrochemical method. **B** TEM image of the TiO_2 sample

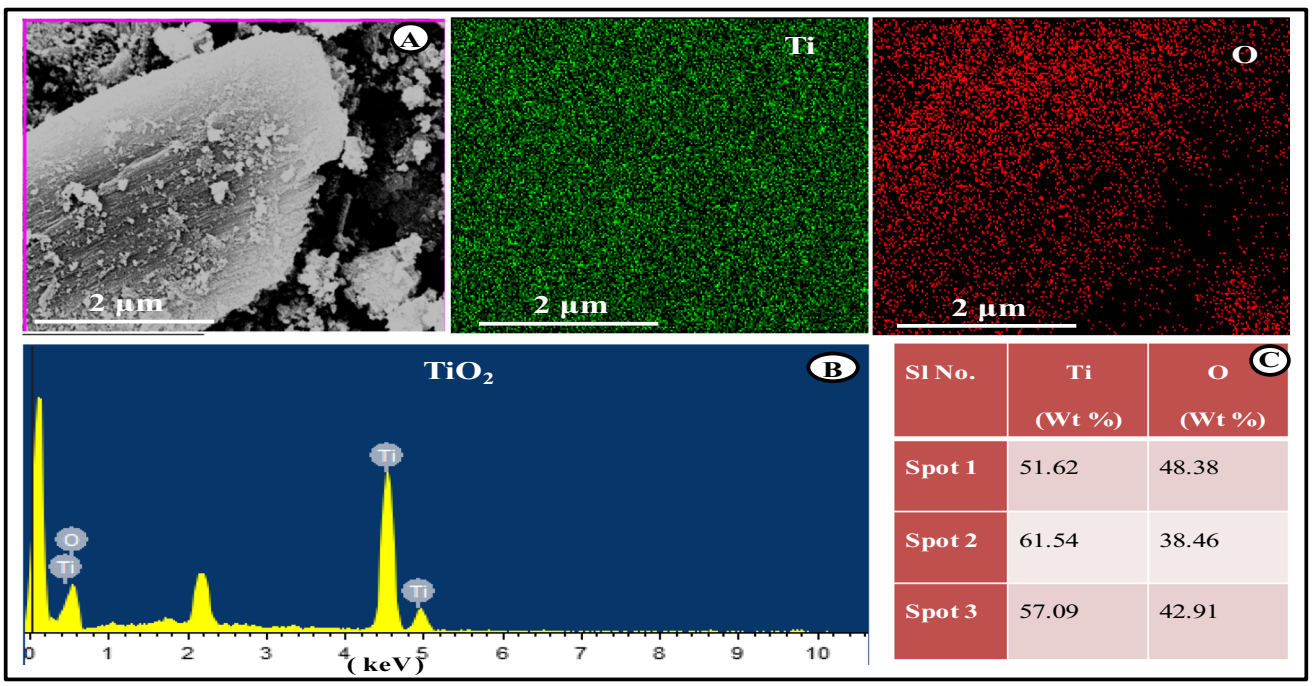

Sl No.	Ti (Wt %)	O (Wt %)
Spot 1	51.62	48.38
Spot 2	61.54	38.46
Spot 3	57.09	42.91

C

Fig. 2 EDX and elemental dot mapping for the purity of TiO_2 nanoparticles

affirmed the high local dispersion of both Ti and O elements over the surface of the catalysts.

The FTIR spectra of the obtained TiO_2 nanoparticles between 4000 and 400 cm^{-1} were taken in ATR mode, as shown in Fig. 3a. The absorption peaks observed at 3019 and 1739 cm^{-1} corresponds to the stretching and bending vibrations of the OH group. The peaks appearing at 1366 and 1219 cm^{-1} are attributed to the COO^- and carboxylic groups bonds resulting from residual succinic acid in the prepared sample. The characteristics band between 800 and 400 cm^{-1} represents the stretching vibrations of Ti–O and Ti–O–Ti bonds which is in agreement with the previous literature (Gomathi Thanga Keerthana et al. 2018).

Powder X-ray diffraction pattern of obtained samples with Miller indices (*hkl*) indicating the crystal family of planes for each diffraction peak is illustrated in Fig. 3b. The sample obtained before calcination shows low intensity, a very broad line centered at about 25° (2θ) indicating amorphous behavior. Whereas the sample obtained after annealed at 500 °C, all diffraction peaks can be attributed to the characteristics of the highly crystalline structure of anatase TiO_2, which perfectly matches with JCPDS card no: 00–004-0477 (Abazari et al. 2014). The lattice parameter observed is $a = b = 3.783$ Å, $c = 9.51$ Å, $\alpha = \beta = \gamma = 90°$, and $V\ (a^2c) = 136.1$ Å3. The intense diffraction peaks appear at Braggs angles (2θ) of 25.35°, 38.50°, 48.07°, 53.92°, 55.12°, 62.72°, 68.59◦, 70.35°, 75.09°, and 83.14° correspond to the crystal planes of (101), (112), (200), (105), (211), (204), (116), (220), (215), and (312) indicate the tetragonal structure of the TiO_2 crystal structure. No diffraction peaks related to secondary phases such as rutile and brookite were observed. The absence of peaks other than TiO_2 confirmed the phase purity of the prepared sample. The Debye–Scherrer equation ($D = K\lambda/\beta \cos\theta$) was utilized to determine the average crystallite size. Where D represents the average crystallite size (Å), K denotes the Scherrer's constant (shape factor) ranging from 0.9 to 1.0, λ is the incident X-ray wavelength (1.54 Å), β denotes the full width at half maxima (FWHM) of the individual XRD peaks, and the diffraction angle is θ. The calculated average mean crystallite size is about 17.42 nm from the major diffraction peak at (101), (112), (200), (105), (211), and (204), where FWHM values are 0.51725, 0.34313, 0.52236, 0.43167, 0.57537, and 0.8195, respectively. The crystallite size changes the electronic properties of the catalyst and plays a vital role in the photoinduced charge separation efficiency within the material. The smaller crystallite size of TiO_2 offers a larger surface area for dye

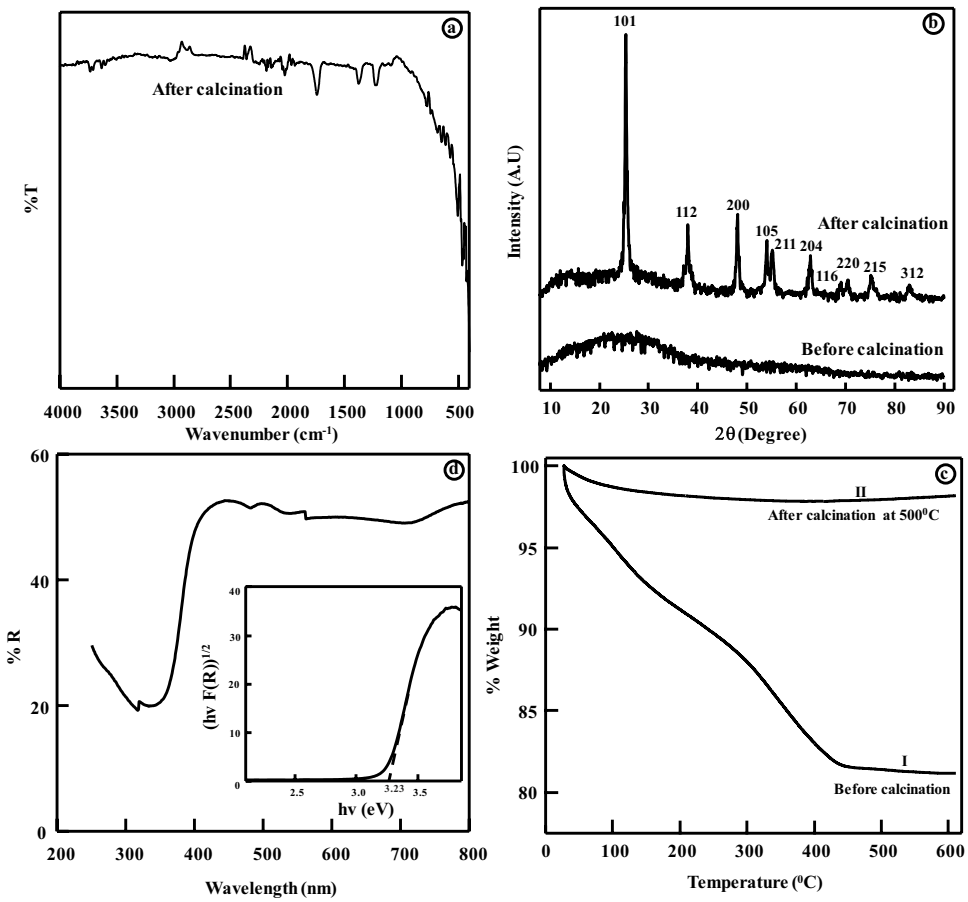

Fig. 3 **a** XRD pattern of prepared TiO_2 nanoparticles before and after calcination at 500 ℃. **b** FTIR spectra of TiO_2 nanoparticles. **c** TGA analysis of nanoparticles before and after calcination. **d** UV–vis diffuse reflectance spectra of calcined TiO_2 nanoparticles. Inset shows the Tauc plot of TiO_2 nanoparticle obtained by electrochemical method

adsorption, which would be beneficial for increasing the photocatalytic efficiency of the catalyst.

TGA analysis was done to analyze the thermal stability of the synthesized TiO_2 nanoparticle. Figure 3c shows the TGA analysis result of before calcination and after calcination of TiO_2 sample. Results for uncalcined TiO_2 exhibits two transition zones from room temperature 27–164 °C and 150–452 °C. The first regime of weight loss of ~ 8% arises due to the removal of water molecules from the obtained sample and the densification of the TiO_2 matrix. The second zone corresponds to ~ 10% weight loss due to the removal of volatile matter present in the sample. The total weight loss was calculated as ~ 18% for the uncalcined sample. TGA of pure TiO_2 nanoparticles obtained at 500 ℃ shows ~ 2% weight loss due to surface moisture content which shows the purity of the material as confirmed by XRD analysis.

The UV–visible diffused reflectance spectra of the synthesized nanomaterial are illustrated in Fig. 3d. The obtained TiO_2 nanoparticle exhibits ~ 53% reflectance in the visible region (420–700 nm) with an absorption edge falling at ~ 340 nm. The absorption in the UV region increases from 47 to 80% due to the absorption and scattering properties of TiO_2 nanoparticles, which is on par with the literature [Li et al. 2015]. The optical band gap E_g is calculated from the following equation $(h\vartheta\alpha)^{\frac{1}{n}} = A(h\vartheta - E_g)$; where $h\vartheta$ represents photon energy of the incident radiation, α denotes the absorption coefficient, E_g implies the optical band gap, and A stands for the absorption coefficient. The exponent n has been taken as 2 to calculate the indirect allowed transition. The absorption coefficient α has been replaced with the Kubelka–Munk function $F(R) = \frac{(1-R)^2}{2R}$ where R denotes the diffused reflectance (Das and Srivastava 2017). Thus the equation can be represented as

$$(h\vartheta F(R))^{\frac{1}{2}} = A\left(h\vartheta - E_g\right)$$

The indirect bandgap of anatase TiO_2 was calculated by converting the absolute reflectance to Kubelka–Munk function and the Tauc plot depicted as an inset in Fig. 3d shows a bandgap of 3.23 eV.

The structural and textural properties of the TiO_2 nanoparticle samples calcined at 500 °C were analyzed by liquid N_2 adsorption–desorption isotherms at 77 K as shown in Fig. 4a. According to IUPAC classification, TiO_2 nanoparticle shows type IV isotherm exhibiting the mesoporous structure of the pores (2–50 nm). The result displays a very small H3 hysteresis loop at a relative pressure range of 0.8–1p/p0. The adsorption at high relative pressures indicates the presence of slit-shaped macropores (plates or edged particles like cubes) in the prepared catalyst. The obtained BET-specific surface area of TiO_2 nanoparticles was 56.34 m^2/g. Barrett–Joyner–Halenda (BJH) adsorption pore size distribution graph is shown in Fig. 4b. BJH pore sizes were calculated from the nitrogen adsorption branches and pore volumes were obtained from the cumulative volume of pores. The pore volume was measured at $^{p}/_{p_0} = 0.99$. The result shows average BJH pore size, pore volume, and pore area are 3.2 nm, 0.0682 cm^3/g, and 37.45 m^2g^{-1}, respectively. Pore volume distribution analysis shows high pore volume in the mesoporous region, which covers the pore diameter range of 2–50 nm. The macroporous region (> 50 nm) illustrates the decreases in pore volume significantly. These mesopores act as the pathways for improving the diffusion and transport of dye molecules on the active site of the catalysts. Thus, the mesoporous nature of catalyst with a large surface area and smaller pore diameter enhanced the photodegradation efficiency (Hosseinpour et al. 2016).

TiO_2 nanoparticles were synthesized by an electrochemical method according to the following reaction:

At anode:

$$Ti \rightarrow Ti^{4+} + 4e^- \tag{3}$$

At cathode:

$$2H_2O + 2e^- \rightarrow H_2 + 2OH^- \tag{4}$$

Reactions exhibited that Ti metal was oxidized in Ti^{4+} as per anodic reaction (3), and hydrogen was generated as per

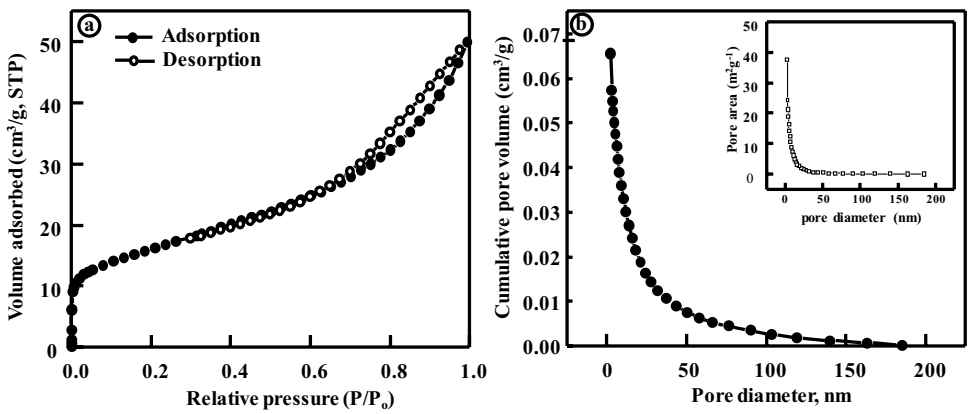

Fig. 4 **a** N_2 adsorption/desorption isotherms of TiO_2 nanoparticle. **b** Pore volume distribution for TiO_2 photocatalysts, where inset shows pore area analysis data

water reduction cathodic reaction (4). During the electrochemical process, dissolution of metal (Ti) from the metallic electrode and corresponding OH radical production via water oxidation method is in confirmation with the literature (Bezares et al. 2015). Furthermore, these metal ions adsorbed produced hydroxyl radicals and formed Ti(OH•). The production of OH ions is mainly depending on the interaction between electrode and electrolyte solution. Again, the surface of the electrode has a significant contribution to the electrochemical and chemical performance of heterogeneous hydroxyl radicals Ti(OH•) and metal oxide (TiO_2) formation as per water oxidation via reaction (5)

$$Ti + H_2O \rightarrow TiO_2 + 4H^+ + 4e- \quad (5)$$

TiO_2 nanoparticle yield synthesized by the electrochemical process was further investigated by varying the operating parameters such as conductivity of electrolyte solution, pH of the solution, reaction time, and applied current. Electrochemical experiments were performed at constant applied current, whereas conductivity varied in the range of 2 to 10 mS/cm. as shown in Fig. 5a. The result shows that with an increase in conductivity, nanoparticle yield increases up to conductivity 6 mS/cm, after that graph shows a plateau value from 6 to 10 mS/cm, and further increases in conductivity productivity decrease. An increase in conductivity increases the current passing through the electrolyte solution, which in turn increase the productivity of nanoparticle, further increase in conductivity nanoparticle production reaches maximum plateau value. After a maximum current production, amorphous titanium dioxide film was formed on the surface of the electrode, which reduces the dissolution rate of titanium surface, and a lesser quantity of titanium ion formation automatically reduces the nanoparticle production (Armstrong 2001).

Figure 5b shows the effect of pH variation on the productivity of the nanoparticle. It has been observed that the nanoparticle yield increases with an increase in pH of the solution up to pH ≈ 7 and gives maximum productivity at pH ≈ 7, after that, it followed a decreasing tendency toward pH ≈ 11. Figure 5c shows the effect of applied current on nanoparticle production. The analysis illustrated that an increase in applied current from 0.05 to 0.2 A increases the TiO_2 nanoparticle yield approximately triple of the initial value after 2 h of reaction. Dissolution of the electrode increases with applied current density in the electrochemical dissolution process (Armstrong 2001), which illustrate the formation of more titanium ion from the anode. Enhanced formation of titanium ions will increase the reaction with an electrolyte solution which in turn improves nanoparticle production. The effect of reaction time on nanoparticle production has been shown in Fig. 5d. The result shows an increase in reaction time productivity of nanoparticles increases. An increase in reaction time produce more number of titanium ion, therefore more number of nanoparticles are produced.

Photocatalytic degradation of rhodamine B

pH of the solution

In photocatalytic degradation reaction, the pH of the pollutant solution is an important factor that pronouncedly

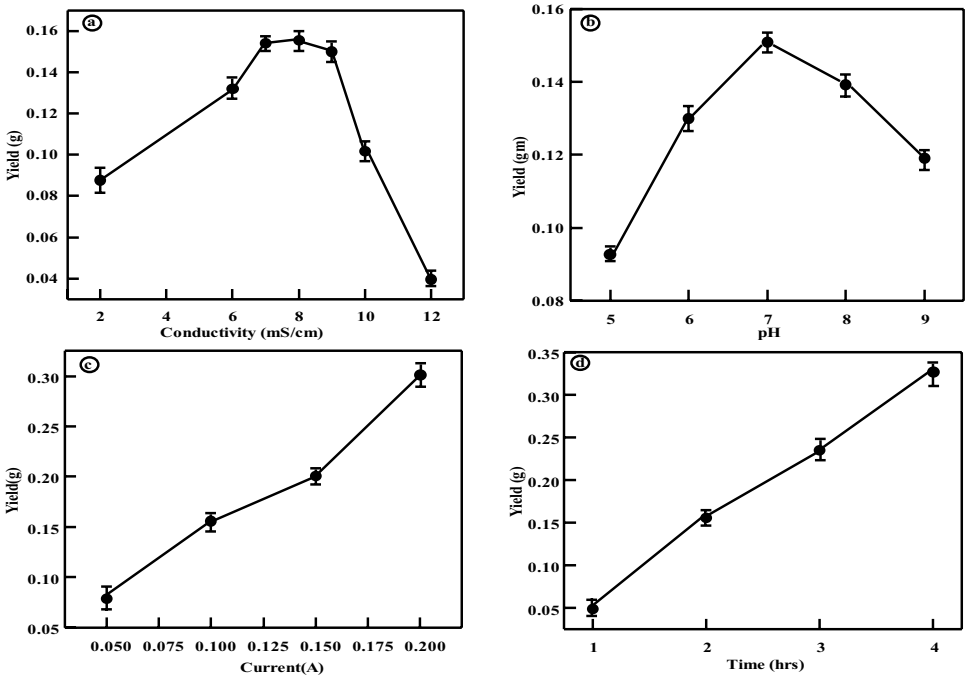

Fig. 5 Effect of various experimental parameters on nanoparticle production **a** Effect of conductivity on nanoparticle production ta 0.1 A current, reaction time 2 h and pH 7. **b** Effect pH at 0.1 A current, reaction time 2 h and conductivity 8. **c** Effect of current at reaction time 2 h, conductivity 8 and pH 7. **d** Effect of reaction time at 0.1 A current, conductivity 8 and pH 7. All experiments were carried out at 0.15 M aqueous succinic acid electrolyte solution

affects the degradation efficiency. The degradation of 5 mg/L RhB dye solution has been studied by using obtained TiO_2 catalyst (1 g/L) under direct sunlight irradiation by varying the pH in the range of 5.5–12 by adjusting with 1 M NaOH solution as shown in Fig. 6a.

The result indicates that the catalytic activity increases with an increase in pH value from the normal to the basic range and allows complete degradation of RhB within 240 min at pH 12. The result shows no significant adsorption (~ 1%) of dye molecules during degradation experiments. This observation illustrates that in an alkaline medium, the production of reactive intermediates such as superoxide hydroxyl radicals increases which in turn enhances the reaction rate. The TiO_2 nanoparticle prepared at 500 °C showed ~ 100% degradation efficiency for pH 12, which is ~ 3 times higher than the normal pH condition. Figure 6b shows the photocatalytic degradation of RhB with different pH values by plotting ln (C/C_0) vs irradiation time (t). The slopes of the plots determine the pseudo-first-order rate constants, k (min^{-1}). It has been observed that the reaction rate constants significantly enhanced from 0.0019 to 0.0224 min^{-1} with an increase in pH value in the basic region. In another word, the reaction rate constant was enhanced by ten times by enhancing the initial pH value of the RhB solution from 5.5 to 12.

Effect of catalyst loading The effect of catalyst loading on dye degradation was investigated by varying TiO_2 catalyst loading from 0.2 to 1 g/L by keeping a constant initial dye concentration (5 mg/L RhB aqueous solution) at pH 12 for all the experiments as shown in Fig. 6c. No significant dye adsorption has been observed due to catalyst loading. The degradation efficiency of the dye solution was increased from 51 to 100% with an increase in catalyst loading from 0.2 to 1 g/L, respectively. An increase in catalyst loading increases the available active sites on the surface of the catalyst for the generation of hydroxyl and superoxide radicals, which increases the degradation rate. The degradation of the dye follows first-order kinetics, and the kinetic parameters are depicted in Fig. 6d for different catalyst loading. The apparent rate constants for the reaction are 0.0035, 0.0057, 0.0079, and 0.0224 mi^{-1} for 0.2, 0.5, 0.7, and 1 g/L catalyst loading, respectively, which illustrated an increase in catalyst loading reaction rate constant also increases.

Effect of initial dye concentration The effect of concentration of initial dye solution was tested by performing degradation experiments with varied dye concentrations from 5 to 50 mg/L at pH 12 and 1 g/L catalyst loading until 240 min light irradiation as shown in Fig. 7a. It has been found that as the initial concentration of the dye increased from 5 to

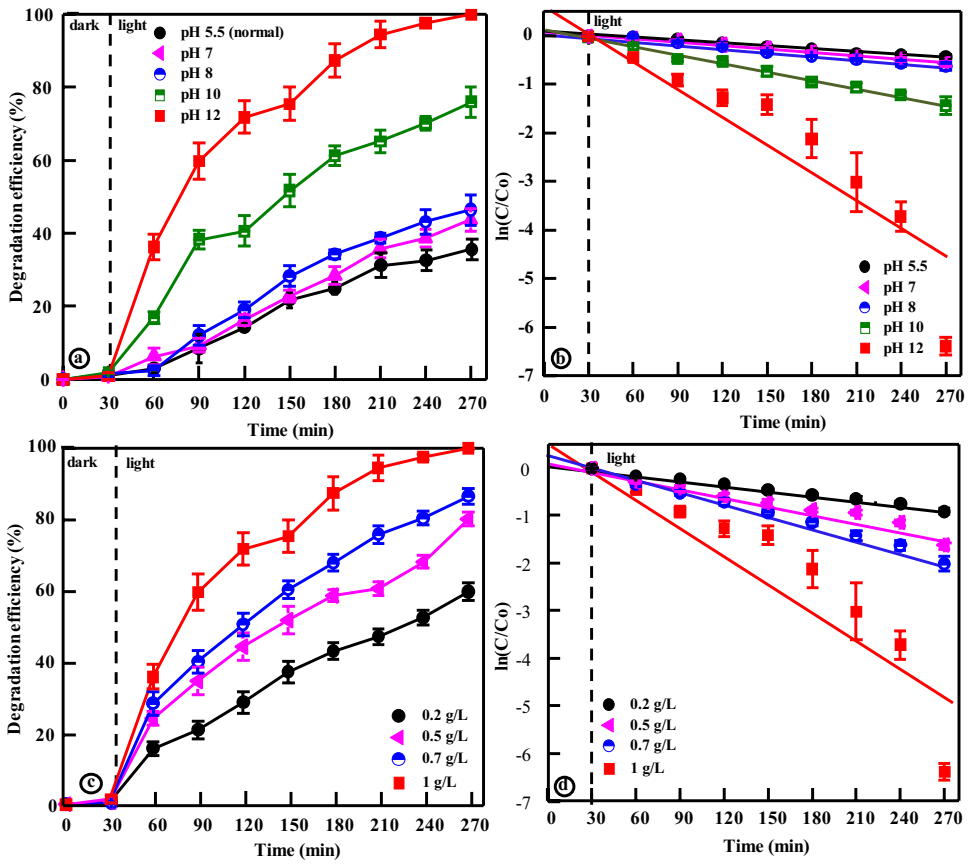

Fig. 6 **a** Effect of initial pH on the photocatalytic degradation efficiency of RhB by TiO_2 catalyst. **b** Reaction kinetic plots of dye degradation at different pH conditions. **c** Effect of different catalyst loading on degradation efficiency. **d** Reaction kinetic plot of RhB degradation by different catalyst loading. The error bars represent the standard deviation of data from several experiments

50 mg/L, the overall photocatalytic degradation efficiency, including the adsorption part, decreased from ~ 100 to 8%. At lower dye concentrations, dye molecules were degraded by superoxide/hydroxyl radicals, which were produced during the excitation of semiconductors by light irradiation. At higher dye concentration, penetration of light within dye solution is more difficult, as a result, the amount of light absorbed on catalyst surface is also decreased, which directly affects the degradation efficiency of dye molecules by reducing the production of superoxide radicals. Dye molecule adsorbed on the catalyst surface for a range of dye concentrations 5 to 50 mg/L was calculated and shown in Fig. 7b. The result shows that with an increase in dye concentration from 5 to 30 mg/L, adsorption of dye molecule also increases from 1 to 6%, after that, it decreases from 6 to 2% with increased dye concentration up to 50 mg/L. A fixed amount of adsorbent can adsorb only a fixed amount of adsorbate species. Due to the availability of vacant pores at the catalyst surface, dye molecules adsorbed rapidly with increasing dye concentration. After reaching a maximum value, the available pores will be blocked by excess dye molecules hence decreasing in the amount of adsorbed dye molecule (Ajmal et al. 2014). The kinetic rate constants for the reaction are 0.0224, 0.0112, 0.0081, 0.0058, 0.0031, and 0.0002 min^{-1} for 5, 20, 30, 40, and 50 mg/L dye loading, respectively. The result illustrates that the reaction rate constant decreases with an increase in initial dye loading concentration.

The decolorization efficiency of RhB at optimum condition was compared with only under dark and only sunlight without catalyst (photolysis) condition as shown in Fig. 8a. Photolysis of RhB shows the degradation of ~ 4% up to light irradiation of 240 min. This result indicates a very weak photolysis degradation of RhB. In dark conditions, the adsorptive removal efficiency was found to be ~ 6%. The absorption spectra of RhB at optimum condition (1 g/L catalyst loading, pH 12, and 5 mg/L dye loading) with different time irradiation have been shown in Fig. 8b. It has been observed that absorption spectra after 30 min adsorption–desorption reaction almost overlapping with the initial spectra, which implies the fact that the catalyst is showing very less absorption (~ 1%) phenomena for RhB degradation. The result shows that the catalyst 100% degrades the dye solution up to light irradiation of 240 min. The overall result shows that TiO_2 catalyst is highly efficient to degrade dye molecules.

The room temperature photoluminescence spectra of the synthesized TiO_2 nanoparticle under an excitation wavelength of 300 nm by Xe lamp have been represented in Fig. 8c. The PL spectra provide information on charge separation and radiative electron–hole recombination efficiency of semiconductors (Khore et al. 2018). The emission peaks of PL are based on the charge carrier density and probability of transition of excited electrons from upper energy state to vacant lower energy state. The result shows the intense broadband in the range 320–550 nm, which is a part of the UV and visible region. The emission peak at 398 nm in the UV region near band edge (NBE) free excitation-emission is attributed to the direct transfer of electrons from the conduction band to the valance band of TiO_2. The peaks that exist in the deep level emission (DLE) band in the visible region provide information related to the site defects present in the TiO_2 sample. The peak adjacent to 412 nm in violet emission is attributed to the presence of defect states on the surface. Peaks near 440 and 460 nm in blue emission depicted the oxygen vacancies and surface defects that occur during electrochemical synthesis. Peaks in the blue-green spectrum (476 and 521 nm) are attributed to the transition of two trapped and one trapped electron from the oxygen vacancies to the valance band of the semiconductor. Strong broadband in the visible region denoted the presence of a large amount of defect in the TiO_2 sample, and all these defects are beneficial for improving photocatalytic properties.

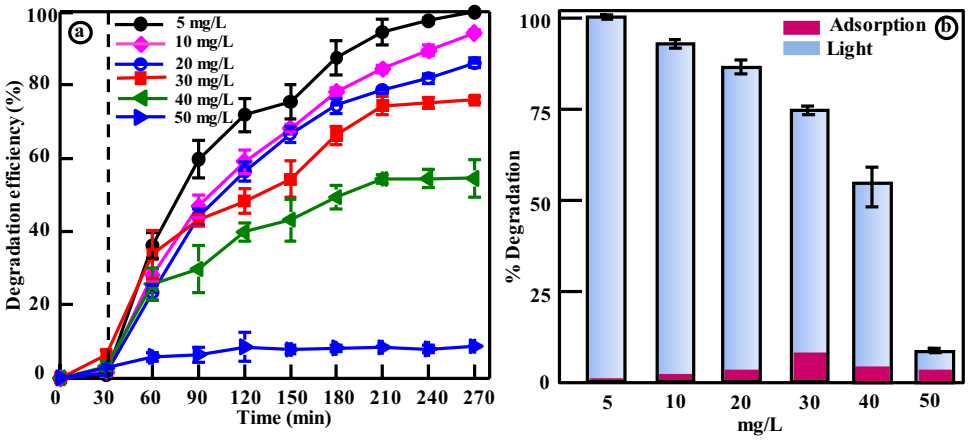

Fig. 7 **a** Effect of initial dye concentration on the degradation of RhB, where the dotted line indicates the adsorption–desorption equilibrium point. **b** Adsorption and photocatalytic degradation efficiency of TiO_2 catalyst

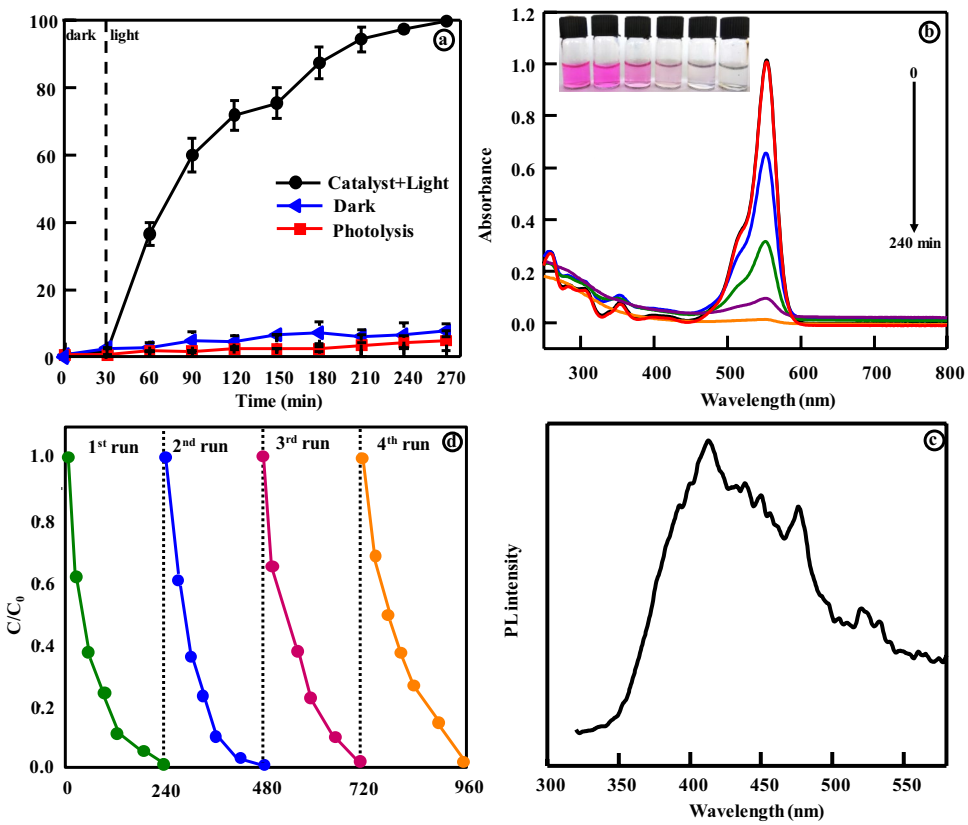

Fig. 8 **a** Degradation of RhB under different conditions (optimum situation, under dark, and photolysis). **b** Time-dependent UV–visible absorption spectra of RhB dye at optimum condition. **c** Recycle test for photocatalytic degradation of RhB by TiO_2 catalyst at optimum condition. **d** Photoluminescence spectra of TiO_2 sample

Stability of the photocatalyst

Besides its photocatalytic activity, the chemical stability of photocatalysts is another significant parameter for its photocatalytic application. To establish the stability of the catalyst, the as-synthesized TiO_2 was recycled by a simple filtration method for RhB dye degradation. Figure 8d shows the degradation of RhB up to 4 cycles using TiO_2 nanoparticles at optimum condition under natural sunlight. After every experiment, TiO_2 catalysts were collected from the solution and washed with deionized water to remove any residual dye from the surface of the nanoparticle. The nanoparticle was then dried in an oven at 60 °C for 12 h. It has been observed from the result that the degradation rate is pretty stable up to 4 cycles. Therefore, TiO_2 may prove to be a beneficial candidate for industrial applications. There is a possibility of catalyst poisoning due to the accumulation of the reaction intermediates on the active site of the catalyst surface during the photocatalytic oxidation process and this poisoning could reduce the efficiency of the catalyst (Saoud et al. 2017). The above result shows that up to 4 recycling, there is no significant change in degradation efficiency, which exhibited no catalyst poisoning. However, there may be a possibility of catalyst poisoning after more recycling processes which could reduce the degradation efficiency.

Mechanism of photodegradation

In the photocatalysis process, semiconductor materials are being excited by incident radiation, which comprises energy more than the bandgap energy of semiconductor materials. After excitation, excited electrons migrate from the valence band to the conduction band of the semiconductor and generate electron–hole pairs which further degrade dye molecules. To estimate the possibility of active species ($O_2^{\bullet-}$, $^{\bullet}OH$) generation over the semiconductor, it is essential to understand the relative positions of the valance and conduction band with respect to the redox potentials of $O_2/O_2^{\bullet-}$ and $^{\bullet}OH/H_2O$. A plausible charge transfer mechanism between TiO_2 and RhB for the degradation of dye has been represented in Fig. 9. The band edges for conduction band (E_{CB}) and valence band (E_{VB}) of a semiconductor are obtained from the following equation (proposed by Butler and Ginley (1978)):

$$E_{CB} = \chi - \frac{1}{2}E_g + E_0 \quad (6)$$

$$E_{VB} = E_{CB} + E_g \quad (7)$$

where χ denotes the Sanderson electronegativity of the semiconductor, the geometric mean of the Mulliken

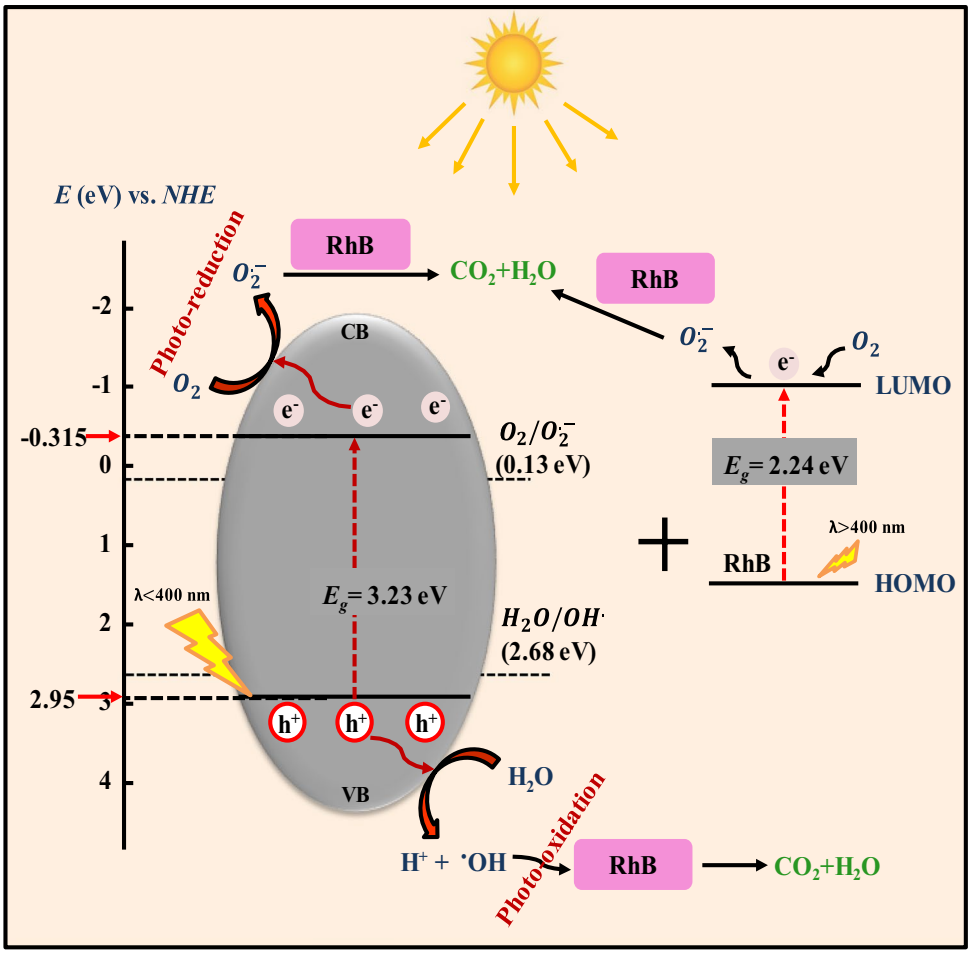

Fig. 9 Schematic presentation of the possible photocatalytic mechanism in terms of energy level diagram of TiO_2 with respect to Energy (vs NHE) of $O_2/O_2^{\bullet-}$ and $\bullet OH/H_2O$ and the HOMO–LUMO energy level of RhB

electronegativities of the constituent atoms. E_g is the bandgap of the semiconductor calculated from the Tauc plot and E_0 is the standard potential of hydrogen in the NHE scale. The Mulliken electronegativity is determined as the arithmetic average of the first ionization energy of the atom and the electron affinity of the formed anion. The ionization energy and electron affinity of Ti are reported as 6.83 and 0.083 eV, and for oxygen, the values are 13.63 and 1.46 eV, respectively (Li et al. 2014). Therefore, the Mulliken electronegativity of Ti and oxygen are found to be 3.45 and 7.54 eV. For a compound notated as M_aX_b, the Sanderson electronegativity can be calculated as per the equation $\chi = (\chi_m^a \chi_x^b)^{\frac{1}{(a+b)}}$ (Yong and Schoonen 2000). Where χ_m and χ_x are the absolute electronegativities of the atoms M and X. The calculated Sanderson electronegativity of TiO_2 is found to be 5.8 eV. The conduction band edge and valance band edge of TiO_2 were estimated to be − 0.315 and 2.915 eV as per Eqs. 6 and 7, respectively. The redox potentials of $^{\bullet}OH/H_2O$ and $O_2/O_2^{\bullet-}$ have been taken as + 0.13 eV vs NHE and 2.68 eV vs NHE, respectively (Kumar et al. 2013).

Since the conduction band edge (− 0.315 eV) of TiO_2 is more negative than the reduction potential of $O_2/O_2^{\bullet-}$, the electrons from the conduction band can react with oxygen molecules and produce superoxide radicals which subsequently take part in the dye degradation. Similarly, holes from the valance band can react with water molecules to produce hydroxyl radicals as the valance band is more positive (2.915 eV) than the electrode potential for the generation of hydroxyl radicals in an aqueous solution. Therefore, the combined action of superoxide and hydroxyl radicals completely mineralize the pollutant leading to the formation of CO_2 and H_2O. The photoexcitation of the electrons results in charge separation, thereby the generation of active species ($O_2^{\bullet-}$,$^{\bullet}OH$, $^{\bullet}OOH$) for the degradation of organic pollutants as follows (Ajmal et al. 2014):

$$TiO_2 + h\vartheta(\lambda < 400\text{nm}) \rightarrow e_{CB}{}^- + h_{VB}{}^+$$

$$H_2O + h_{VB}{}^+ \rightarrow {}^{\cdot}OH + H^+$$

$$O_2 + e_{CB}{}^- \rightarrow O_2^{\cdot-}$$

$$O_2^{\cdot-} + H^+ \leftrightarrow {}^{\cdot}OOH$$

$$2HOO^{\cdot} \rightarrow H_2O_2 + O_2$$

$$H_2O_2 \rightarrow 2^{\cdot}OH$$

$$RhB + h\vartheta(\lambda > 340nm) \rightarrow RhB^{+}(excitedstate)$$

$$RhB^{+} \rightarrow CO_2 + H_2O$$

$$RhB^{+} + (O_2^{-\cdot}, {}^{\cdot}OH, {}^{\cdot}OOH) \rightarrow intermediates \rightarrow CO_2 + H_2O$$

The UV fraction of the natural sunlight spectrum ($\lambda < 400nm$) is responsible for the photocatalytic activity of TiO_2 nanoparticles. In addition, under visible light irradiation ($\lambda > 400nm$), the dye in bulk solution changes from the ground state to an excited state, and the excited state of the dye reacts with the dissolved oxygen in the aqueous solution giving rise to the generation of active oxygen species which further degrades the dye.

$$RhB \xrightarrow{h\vartheta} RhB^{*}$$

$$RhB^{*} + O_2 \rightarrow RhB^{\cdot+} + O_2^{-\cdot}$$

$$O_2^{-\cdot} + H^{+} \rightarrow OOH^{\cdot}$$

$$OOH^{\cdot}/O_2^{-\cdot} + RhB \rightarrow Degradedproducts$$

In general, hole (h^+), superoxide radical ($O_2^{\bullet-}$), and hydroxyl radical ($^{\bullet}OH$) are always considered the key reactive species involved in the photocatalytic degradation process. To confirm the major active species involved in the degradation process, a scavenger study was carried out by adding 6 mM of different scavengers such as ethylene diamine tetra-acetic acid (EDTA, h^+ quencher), isopropyl alcohol (IPA, $^{\bullet}OH$ quencher), and ascorbic acid (AA, $O_2^{\bullet-}$ quencher) to the photocatalytic system. Figure 10 shows the degradation profile of RhB up to an irradiation time of 240 min under the optimum condition with and without scavengers. The result illustrated that in the presence of EDTA and AA, the degradation efficiency of RhB was highly suppressed, and the photocatalytic degradation rates were only ~ 23 and 5%, respectively. The addition of IPA has very less suppression with a dye degradation efficiency of ~ 85%. It has been observed that the decrease in the removal rate in the presence of scavengers presents the following trend: AA > EDTA > IPA. Results illustrated that the hole and superoxide radicals acted as dominant active species for photocatalytic degradation of RhB under visible light irradiation. Thus, it can be inferred that the holes and superoxide radicals acted as dominant active species for photocatalytic degradation of RhB under visible light irradiation.

Adsorption study of rhodamine B

During the photocatalytic experiments of RhB, the mixture of dye solution and catalyst was placed under dark with stirring for 30 min to attain the adsorption–desorption equilibrium at room temperature. The result showed very poor dye adsorption in the case of RhB dye solution. At optimum experimental conditions (pH 12 and 1 g/L catalyst loading), varying initial dye concentration from 5 to 50 mg/L shows maximum adsorption of ~ 6%, as shown in Fig. 7. For a better understanding of the adsorption process, we have performed the adsorption experiments in detail.

The adsorption isotherm of RhB dye was investigated over a range of RhB dye concentrations from 5 to 30 ppm at four different temperatures of 30, 40, 45, and 55 °C. All the experiments were carried out at 5 g/L catalyst loading, pH 12, and a fixed contact time of 60 min. In this study, the Langmuir and Freundlich isotherm models were tested to understand the adsorption mechanism. The adsorption

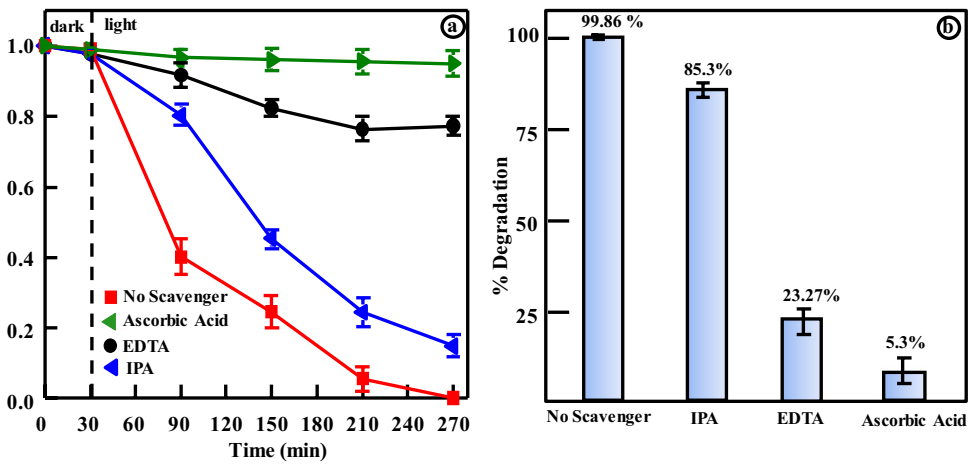

Fig. 10 **a** Photocatalytic degradation of RhB in the presence of scavengers. **b** Effect of a different scavenger of degradation of RHB

parameters were calculated by using the following linear form of the Langmuir isotherm model:

$$\frac{1}{q_e} = \frac{1}{q_m k_L C_e} + \frac{1}{q_m} \tag{8}$$

where C_e, q_e, and q_m represent the equilibrium concentration of RhB (mg/L), the amount of mass of RhB absorbed per gram of adsorbent at equilibrium concentration (mg/g), and the maximum adsorption capacity, respectively. K_L denotes the Langmuir constant (L/mg) (Dinh et al. 2019, Raghav et al. 2018).

The linear form of the Freundlich adsorption isotherms model is represented by

$$\ln q_e = \ln K_f + \frac{1}{n}\ln C_e \tag{9}$$

where K_f is Freundlich's constant and is used to measure the adsorption capacity. "n" denotes the adsorption intensity, which is useful to determine the adsorption trend. $n = 1$ indicate the linear adsorption,$n < 1$ is an indication of chemical adsorption and unfavorable and $n > 1$ is a representation of physical adsorption and favorable (Al-Ghouti and Al-Absi 2020). The parameters of the adsorption isotherm with the corresponding coefficient of determination (R^2) values are tabulated in Table 1.

The parameters of the adsorption isotherm with the corresponding coefficient of determination (R^2) values are tabulated in Table 1. The calculated R^2 values are close to 1 for both the isotherms, which validates the applicability for both the isotherms. Specifically, R^2 values are slightly higher for the Langmuir isotherm than those obtained from the Freundlich isotherm model at 45 and 55 °C, although the difference are very small. These small difference in R^2 values at 45 and 55 °C suggest that the Langmuir isotherm model is slightly better fitting than the Freundlich isotherm model, thus indicating the formation of a monolayer of RhB dye on a homogeneous surface (Dinh et al. 2019).

In the Langmuir isotherm model, the dimensionless constant is known as separation factor (R_L) was calculated from the following equation (Raghav et al. 2018; Maruthapandi et al. 2018):

$$R_L = \frac{1}{1 + K_L C_0} \tag{10}$$

where C_0(mg/L) and K_L(L/mg) represent the initial RhB concentration and Langmuir equilibrium constant, respectively. The value of R_L is larger than 1 indicates the unfavorable process, R_L equal to 1 implies the linear process, R_L is equal to zero means irreversible process, and R_L is within a range of 0 to 1 corresponds to a favorable process. In our analysis, the values of R_L are found to be within a range of 0.408–0.858 for RhB adsorption, which indicates the favorable adsorption of RhB onto adsorbents. On the other hand, the analysis revealed that the values of "n" are within a range of 1.35 to 1.43. According to the result, the higher values of "n," which lies in between 1 and 10, represent that the RhB dye adsorption process onto TiO_2 catalyst is a favorable physical process. This is consistent with the result of the Langmuir model.

Table 1 Parameters for the equilibrium models at different temperatures

Isotherm models	Parameters	Temperature (°C)			
		30	40	45	55
Langmuir	q_m (mg/g)	1.1375	1.6625	2.2502	2.3855
	K_L (L/mg)	0.0483	0.0414	0.0329	0.0362
	R^2	0.9765	0.9967	0.9976	0.9945
Freundlich	K_F (L/mg)	0.0678	0.0933	0.0978	0.1162
	n	1.3945	1.4310	1.3563	1.3972
	R^2	0.9702	0.9925	0.9784	0.9825

Effect of temperature on RhB adsorption

The effect of temperature on RhB adsorption was studied by carrying out the adsorption experiments at 5 g/L catalyst loading, pH 12, and a fixed contact time of 60 min at four different temperatures of 30, 40, 45, and 55 °C, as shown in Fig. 11. Experimental result shows that the adsorption capacity q_e increases with an increase in temperature which indicates the higher temperature is favorable for the adsorption process (Fu et al. 2015; Mushtaq et al. 2016). The possible explanation could be, at the higher temperature, intraparticle diffusion increases, which boosts up the adsorption phenomenon (Fu et al. 2015).

Thermodynamic study

In order to describe the thermodynamic behavior of adsorption of RhB, the adsorption experiments were performed over a range of RhB dye concentrations from 5 to 30 ppm at four different temperatures of 30, 40, 45, and 55 °C. All the experiments were carried out at 5 g/L catalyst loading, pH 12, and a fixed contact time of 60 min. The thermodynamic parameters for the adsorption process such as a change in Gibbs free energy (ΔG), enthalpy (ΔH), and entropy (ΔS) were evaluated in the temperature range 30 to 55 °C from the following equations (Liu 2009; Lima et al. 2019):

$$\Delta G = -RT\ln(K_L)$$

$$\Delta G = \Delta H - T\Delta S$$

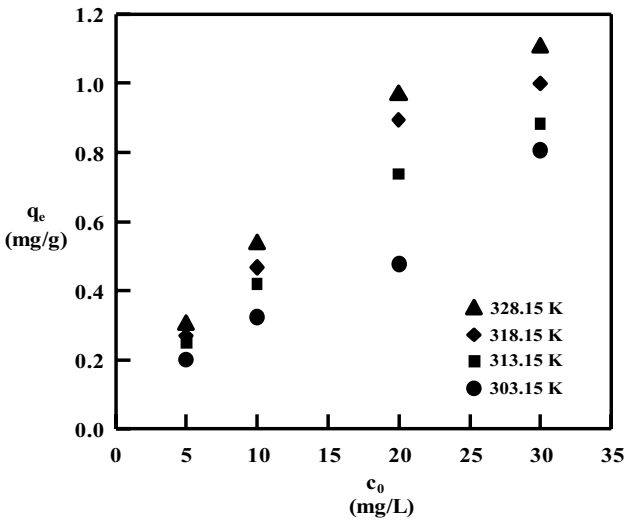

Fig. 11 Effect of temperature on the adsorption of RhB onto TiO2 surface

Table 2 Thermodynamic parameter for adsorption of RhB onto TiO_2 at different temperatures

T (°K)	ΔG (kJ/mol)	ΔS (J/mol.K)	ΔH (kJ/mol)
303.15	− 25.63	47.56	− 10.82
313.15	− 26.09		
318.15	− 25.87		
328.15	− 26.94		

$$\ln(K_L) = \Delta S/R - \Delta H/RT$$

where K_L represent the Langmuir equilibrium constant (L/mol), R denotes the universal gas constant (8.314 J/mol K), and T refers to the absolute temperature (K). The values of the thermodynamic parameters obtained from the adsorption process are presented in Table 2. The analysis shows that the calculated ΔG values were found to be negative, which indicates the spontaneous nature of the adsorption process. A similar type of result has also been reported by previous researchers (Dinh et al. 2019). The negative ΔH value represents that the Rhodamine B adsorption process is exothermic (Noreen et al. 2020). The positive ΔS value suggests some structural changes in the TiO_2 adsorbent and RhB and the increasing randomness at the solid-solution interface during fixation of RhB onto the active sites of TiO_2 (Fu et al. 2015). Overall, the thermodynamics parameters illustrated that the adsorption process is spontaneous and exothermic.

The analysis shows that the adsorption capacity q_e (mg/g) values are very less (0.2 to 1.11 mg/g) for the RhB adsorption onto obtained TiO_2 catalyst. Thus, the result represents that the adsorption of RhB onto TiO_2 nanoparticles is poor, which we have already mentioned in the result of adsorption–desorption of photocatalytic degradation experiments. In the literature also, researchers have shown anatase TiO_2 as a very poor adsorbent which is in agreement with our result (Niu et al. 2021).

In summary, the degradation of RhB dye was mainly dominated by the photocatalytic activity of catalyst rather than the adsorption process. The overall performance of a photocatalyst is collectively determined by many interrelated parameters. In the present work, the crystallinity, crystallite size, surface area, pore size distribution, presence of oxygen vacancies, and defect states in the TiO_2 play a key role in the photocatalytic efficiency of TiO_2 nanoparticles. It is evident from the literature that high crystallinity provides a better charge diffusion pathway for electron transfers from the conduction band of the material to the active sites, hence the high crystallinity of the prepared TiO_2 material has a significant impact on the photocatalytic activity. Similarly, a smaller crystallite size of TiO_2 provides better adsorption of the pollutants onto the crystallite surface. A large surface area with mesoporous nature and wide pore size distribution help in the diffusion of pollutants to the interior of the pores and subsequent adsorption in the active sites providing better photodegradation. The presence of oxygen vacancies and surface defects, as demonstrated in the PL spectra, confirms the better charge separation in the material by suppressing the charge recombination enhance the degradation process. Furthermore, the photocatalysis process was aided by the operating parameters such as pH, catalyst dosage, and initial concentration of the dye.

Conclusion

In summary, we demonstrated a cost-effective, simple electrochemical technique to synthesize TiO_2 nanoparticles where succinic acid was used as a non-ammonia-based aqueous electrolyte solution. Various characterization techniques XRD, FTIR, SEM, TEM, BET, and UV-DRS confirm the anatase phase of tetragonal TiO_2 nanoparticles of ~ 40 nm diameter. The result showed that the productivity of the TiO_2 nanoparticle could be maximized by increasing experimental parameters such as applied current and reaction time at an optimum pH and conductivity. The adsorption study of RhB onto TiO_2 nanoparticles exhibited poor adsorption capacity for RhB. Photocatalysis analysis revealed that factors like pH of the solution, catalyst loading, and dye concentration have a significant effect on the RhB photodegradation process. At the optimum experiment conditions of pH 12 and 1 g/L catalyst loading, ~ 100% degradation of 5 mg/L RhB was noticed in 240 min where the degradation process followed a first-order reaction kinetics with an apparent rate constant of 0.0224 min^{-1}. The crystallinity, crystallite size, surface area, pore size distribution, presence of oxygen vacancies, and

defect states in the TiO_2 play a key role in the photocatalytic efficiency of TiO_2 nanoparticles. Furthermore, the photocatalysis process was aided by the operating parameters such as pH, catalyst dosage, and initial concentration of the dye under natural sunlight. Efficient photocatalytic degradation of RhB under natural sunlight shows its good opportunity in future application in degrading various other organic pollutants as well as industrial wastewater treatment. Stability experiments and scavenger study of RhB degradation showed that the TiO_2 remains highly photocatalytic active and stable for a long time duration. Thus, it is expected that this TiO_2 catalyst can be a low-cost and environment-friendly promising candidate for natural sunlight-driven photocatalytic application in industrial effluent treatment.

Author contribution S. Das conceived the original idea, planned, and supervised the work. S. Das and S. Vishwanathan drafted the initial manuscript and were involved in conducting all the experiments. Sree-Laxmi, S. Nandan, S. Jayan, and M. Lijo have conducted initial few experiments. All authors read and approved the final manuscript.

Funding The author wishes to acknowledge the Science and Engineering Research Board of New Delhi, India, for financial support to carry out this work under Project No. SRG/2019/001732. The Faculty Research Grant (NITC/DEAN(R&C)/ FRG/2018–19) by the National Institute of Technology Calicut, India. Technical Education Quality Improvement Program (TEQIP-III) fund by National Institute of Technology Calicut, India.

Data Availability The authors declare that all data related to this study are available within this article.

Code availability Not applicable.

Declarations

Ethics approval and consent to participate Not applicable.

Consent for publication Not applicable.

Conflict of interest The authors declare no competing interests.

References

Abazari R, Mahjoub AR, Sanati S (2014) A facile and efficient preparation of anatase titania nanoparticles in micelle nanoreactors: morphology, structure, and their high photocatalytic activity under UV light illumination. RSC Adv 4(99):56406–56414. https://doi.org/10.1039/c4ra10018b

Al-Ghouti MA, Al-Absi RS (2020) Mechanistic understanding of the adsorption and thermodynamic aspects of cationic methylene blue dye onto cellulosic olive stones biomass from wastewater. Sci Rep 10:15928. https://doi.org/10.1038/s41598-020-72996-3

Ajmal A, Majeed I, Malik RN, Idriss H, Nadeem MA (2014) Principles and mechanisms of photocatalytic dye degradation on TiO_2 based photocatalysts: a comparative overview. RSC Adv 4(70):37003–37026. https://doi.org/10.1039/c4ra06658h

P Anandgaonker G Kulkarni S GaikwadA Rajbhoj 2015 Synthesis of TiO2 nanoparticles by electrochemical method and their antibacterial application Arab J Chem 0–7 https://doi.org/10.1016/j.arabjc.2014.12.015

RD Armstrong 2001 Electrochemical dissolution Encycl Mater Sci Technol 2521–2525 https://doi.org/10.1016/b0-08-043152-6/00456-3

Bezares I, Del Campo A, Herrasti P, Munoz-Bonilla A (2015) A simple aqueous electrochemical method to synthesize TiO_2 nanoparticles. Phys Chem Chem Phys 17(43):29319–29326. https://doi.org/10.1039/c5cp05525c

Butler MA, Ginley DS (1978) Prediction of flatband potentials at semiconductor-electrolyte interfaces from atomic electronegativities. J Electrochem Soc 125(2):228–232. https://doi.org/10.1149/1.2131419

Carter, C. B., & Norton, M. G. (Eds.). (2007). Sols, gels, and organic chemistry. In Ceram Mater Sci Eng (pp. 400–411). New York, NY: Springer. https://doi.org/10.1007/978-0-387-46271-4_22

V Santo Dal ANaldoni 2018 Titan Dioxide Photocatal Catal 8 12 591 https://doi.org/10.3390/catal8120591

Das S, Srivastava VC (2017) Synthesis and characterization of ZnO/CuO nanocomposite by electrochemical method. Mater Sci Semicond Process 57:173–177. https://doi.org/10.1016/j.mssp.2016.10.031

V-P Dinh T-D-T Huynh HM Le V-D Nguyen Dao, V-Ai., N. Q. Hung, Tuyen, L. A., Lee, S., Yi, J., Nguyen, T. D., Tan, L. V. 2019 Insight into the adsorption mechanisms of methylene blue and chromium(III) from aqueous solution onto pomelo fruit peel RSC Adv 9 25847 https://doi.org/10.1039/C9RA04296B

Dong H, Chen YC, Feldmann C (2015) Polyol synthesis of nanoparticles: status and options regarding metals, oxides, chalcogenides, and non-metal elements. Green Chem 17(8):4107–4132. https://doi.org/10.1039/c5gc00943j

Filippo E, Carlucci C, Capodilupo AL, Perulli P, Conciauro F, Corrente GA et al (2015) Facile preparation of TiO_2–polyvinyl alcohol hybrid nanoparticles with improved visible light photocatalytic activity. Appl Surf Sci 331:292–298. https://doi.org/10.1016/j.apsusc.2014.12.112

Fu J, Chen Z, Wang M, Liu S, Zhang J, Zhang J, Han R, Xu Q (2015) Adsorption of methylene blue by a high-efficiency adsorbent (polydopamine microspheres): kinetics, isotherm, thermodynamics and mechanism analysis. Chem Eng J 259:53–61. https://doi.org/10.1016/j.cej.2014.07.101

GT Keerthana B., Solaiyammal, T., Muniyappan, S., & Murugakoothan, P 2018 Hydrothermal synthesis and characterization of TiO2 nanostructures prepared using different solvents Mater Lett 220 20 23 https://doi.org/10.1016/j.matlet.2018.02.119

Guimaraes de Oliveira A, Nascimento JP, de Fatima Gorgulho H, Martelli PB, Furtado CA, Figueiredo JL (2016) Electrochemical synthesis of TiO_2/graphene oxide composite films for photocatalytic applications. J Alloy Compd 654:514–522. https://doi.org/10.1016/j.jallcom.2015.09.110

A Hajjaji M Elabidi K Trabelsi K., Assadi, A.A., Bessais, B., Rtimi, S. 2018 Bacterial adhesion and inactivation on Ag decorated TiO2-nanotubes under visible light: effect of the nanotubes geometry on the photocatalytic activity Colloids Surf, B 170 92 98 https://doi.org/10.1016/j.colsurfb.2018.06.005

Hosseinpour Z, Hosseinpour S, Maaza M, Scarpellini A (2016) Co^{2+} and Ho^{3+} doped CuS nanocrystals with improved photocatalytic activity under visible light irradiation. RSC Adv 6(48):42581–42588. https://doi.org/10.1039/c6ra03647c

OL Kang A Ahmad UA Rana NH Hassan 2016 Sol-gel titanium dioxide nanoparticles: preparation and structural characterization J Nanotechnol 2016 https://doi.org/10.1155/2016/5375939

Khore SK, Kadam SR, Naik SD, Kale BB, Sonawane RS (2018) Solar light active plasmonic Au@TiO_2 nanocomposite with superior

photocatalytic performance for H2 production and pollutant degradation. New J Chem 42(13):10958–10968. https://doi.org/10.1039/c8nj01410h

Kumar S, Surendar T, Baruah A, Shanker V (2013) Synthesis of a novel and stable g-C_3N_4-Ag_3PO_4 hybrid nanocomposite photocatalyst and study of the photocatalytic activity under visible light irradiation. J Mater Chem A 1(17):5333–5340. https://doi.org/10.1039/c3ta00186e

L Li PA Salvador GS Rohrer 2014 PhotocatalInt Electric Fields Nanoscale 6 1 24 42 https://doi.org/10.1039/c3nr03998f

Lima EC, Hosseini-Bandegharaei A, Moreno-Piraján JC, Anastopoulos I (2019) Critical review of the estimation of the thermodynamic parameters on adsorption equilibria. Wrong use of equilibrium constant in the Van't Hoof equation for calculation of thermodynamic parameters of adsorption. J Mol Liq 273:425–434. https://doi.org/10.1016/j.molliq.2018.10.048

Liu Y (2009) Is the free energy change of adsorption correctly calculated? J Chem Eng Data 2009(54):1981–1985. https://doi.org/10.1021/je800661q

Li X, Fang Y, Hu Y, Huo H, Zhao S, Long X, Ma J, Li R (2015) Mesoporous titanium dioxide coating on gold modified silica nanotubes: a tube-in-tube titanium nanostructure for visible-light photocatalysts. RSC Adv 5(2015):69962–69969. https://doi.org/10.1039/c5ra11934k

Maruthapandi M, Kumar VB, Luong JHT, Gedanken A (2018) Kinetics, isotherm, and thermodynamic studies of methylene blue adsorption on polyaniline and polypyrrole macro−nanoparticles synthesized by c-dot-initiated polymerization. ACS Omega 3:7196–7203. https://doi.org/10.1021/acsomega.8b00478

Mushtaq M, Bhatti HN, Iqbal M, Noreen S (2016) Eriobotrya japonica seed biocomposite efficiency for copper adsorption: isotherms, kinetics, thermodynamic and desorption studies. J Environ Manage 176:21–33. https://doi.org/10.1016/j.jenvman.2016.03.013

Nakata K, Fujishima A (2012) TiO_2 photocatalysis: design and applications. J Photochem Photobiol, C 13(3):169–189. https://doi.org/10.1016/j.jphotochemrev.2012.06.001

Niu L, Zhao X, Tang Z, Lv H, Wu F, Wang X, Zhao T, Wang J, Wu A, Giesy JP (2021) Difference in performance and mechanism for methylene blue when TiO_2 nanoparticles are converted to nanotubes. J Clean Prod 297:126498. https://doi.org/10.1016/j.jclepro.2021.126498

Noreen, S., Khalida, U., Ibrahimb, S. M., Javedd, T., Ghanie, A., Nazf, S., Iqbalg, M. (2020). ZnO, MgO and FeO adsorption efficiencies for directsky blue dye: equilibrium, kinetics andthermodynamics studies, J Mater Res Technol l 9, 5881–5893. https://doi.org/10.1016/j.jmrt.2020.03.115

Pan, L., Zou, J., Liu, X., Liu, X., Wang, S., Zhang, X., & Wang, L. (2012). Visible − light − induced photodegradation of rhodamine b over hierarchical TiO_2 : effects of storage period and water-mediated adsorption switch. 51(39), 12782–12786. https://doi.org/10.1021/ie3019033

Raghav S, Kumar D (2018) Adsorption equilibrium, kinetics, and thermodynamic studies of fluoride adsorbed by tetrametallic oxide adsorbent. J Chem Eng Data 2018(63):1682–1697. https://doi.org/10.1021/acs.jced.8b00024

Rane, A. V., Kanny, K., Abitha, V. K., & Thomas, S. (2018). Chapter 5 - methods for synthesis of nanoparticles and fabrication of nanocomposites. In S. Mohan Bhagyaraj, O. S. Oluwafemi, N. Kalarikkal, & S. Thomas (Eds.), Synth Inorgan Nanomater (pp. 121–139). Woodhead Publishing. https://doi.org/10.1016/B978-0-08-101975-7.00005-1

Roy P, Berger S, Schmuki P (2011) TiO_2 Nanotubes: synthesis and applications. Angew Chem Int Ed 50(13):2904–2939. https://doi.org/10.1002/anie.201001374

Sankapal BR, Sartale SD, Lux-Steiner MC, Ennaoui A (2006) Chemical and electrochemical synthesis of nanosized TiO_2 anatase for large-area photon conversion. C R Chim 9(5):702–707. https://doi.org/10.1016/j.crci.2005.06.035

Saouda, W. A., Assadia, A. A., M Guizab, M., Bouzazaa, A. Aboussaoudb,W., Ouedernib, A., Soutrela, I., Wolberta, D., Rtimi, S. (2017) Study of synergetic effect, catalytic poisoning and regeneration usingdielectric barrier discharge and photocatalysis in a continuousreactor: abatement of pollutants in air mixture system Appl Catal B: Environ 213 53–61. http://dx.doi.org/https://doi.org/10.1016/j.apcatb.2017.05.012

Tripathy SK, Sahoo T, Mohapatra M, Anand S, Yu YT (2009) Polyol-assisted synthesis of TiO_2 nanoparticles in a semi-aqueous solvent. J Phys Chem Solids 70(1):147–152. https://doi.org/10.1016/j.jpcs.2008.09.013

Yong X, Schoonen MAA (2000) The absolute energy positions of conduction and valence bands of selected semiconducting minerals. Am Miner 85(3–4):543–556. https://doi.org/10.2138/am-2000-0416

Zeghioud, H., Kamagateb, H. M., Coulibalyd, L S., Rtimi, S., Assadib, A. A. (2019). Photocatalytic degradation of binary and ternary-mixtures of antibiotics: reactive species investigation in pilot scale. Chem Eng Res Des 1 4 4, 300–309. https://doi.org/10.1016/j.cherd.2019.02.015

H Zeghioud AA Assadic N Khellafa H Djelald A Amranec S Rtimi S 2018 Reactive Species Monitoring and Their Contribution for Removal of Textile Effluent with Photocatalysis under UV and Visible Lights: DynMech J Photochem Photobiol A: Chem 365 94 102 https://doi.org/10.1016/j.jphotochem.2018.07.031